Journal of Materials Chemistry A

Accepted Manuscript

This article can be cited before page numbers have been issued, to do this please use: J. Cheng, H. Zhang, S. Zhang, D. Ouyang, Z. Huang, M. K. Nazeeruddin, J. Hou and W. C.H. Choy, *J. Mater. Chem. A*, 2018, DOI: 10.1039/C8TA08819E.

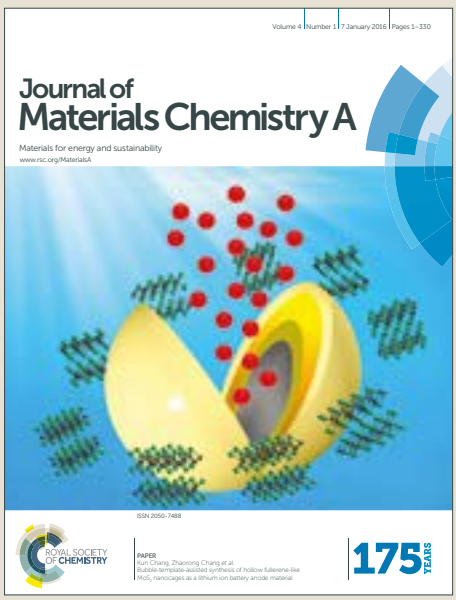

ROYAL SOCIETY OF CHEMISTRY

rsc.li/materials-a

DOI: 10.1039/C8TA08819E

Highly Efficient Planar Perovskite Solar Cells Achieved by Simultaneous Defect Engineering and Formation Kinetic Control

*Jiaqi Cheng#, Hong Zhang#, Shaoqing Zhang, Dan Ouyang, Zhanfeng Huang, Mohammad Khaja Nazeeruddin, Jianhui Hou, Wallace C. H. Choy**

Dr. J. Cheng, Dr. H. Zhang, D. Ouyang, Z. Huang, Prof. W. C. H. Choy
Department of Electrical and Electronic Engineering
The University of Hong Kong
Pokfulam Road, Hong Kong, China
E-mail: chchoy@eee.hku.hk

Dr. S. Zhang, Prof. J. H. Hou
Institute of Chemistry
Chinese Academy of Sciences
Beijing 100190, China

Prof. M.K. Nazeeruddin
Group for Molecular Engineering of Functional Materials
Institute of Chemical Sciences and Engineering
École Polytechnique Fédérale de Lausanne
CH-1951 Sion, Switzerland.

# Contributed equally to the work

Keywords: perovskite, cyano, formation kinetic, solar cells, defect

Abstract

The formation of high quality (good morphology and low defect concentrations) perovskite films is crucial for realizing high-performance perovskite solar cells (PVSCs). Low-temperature processed perovskite films tend to have a high density of defect states, which hinder the enhancement of their device performance. Although various post-treatment methods have been reported to passivate the surface defects of perovskite, the critical issue is that defects inside the bulk film cannot be passivated simultaneously. Here, we demonstrate a new strategy of simultaneously controlling the perovskite formation kinetics and reducing the defects (e.g., unsaturated Pb) for achieving densely packed perovskite films with low defect concentrations. The strategy is realized through incorporating cyano-based small molecules into perovskite precursor. Our results show that the inverted planar-structured PVSCs with the perovskite films formed by the new strategy have significant performance improvement with PCE reaching 20.10%, which is among the highest values of low-temperature processed solar cells. This work provides a new strategy to further improve the quality of low-temperature processed perovskite films and the relevant device performances.

TOC

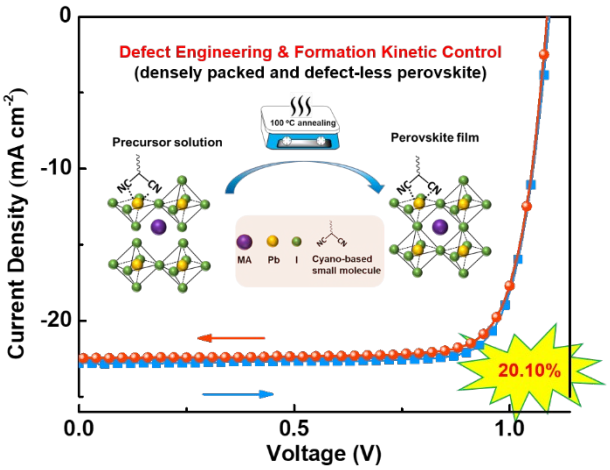

1. Introduction

Perovskite solar cells (PVSCs) have attracted intensive attention due to their merits of high performance and low-cost fabrication.[1] Although the certified power conversion efficiency (PCE) of PVSCs has reached 22.7%,[2] defect states and localized electronic states causing non-radiative carrier recombination have been the critical concern for further development of PVSCs.[3] The dangling bonds or non-coordination atoms exist at the boundary of perovskite crystals would also act as the carrier recombination centers and contribute to carrier recombination in PVSCs.[4] For instance, a recombination kinetics investigation on methylammonium lead bromide ($MAPbBr_3$) single crystal has discerned that the surface trap density (6.0×10^{17} cm^{-3}) is two orders larger than that of the bulk (5.8×10^{15} cm^{-3}).[5] Moreover, the defect-assisted trapping has been also reported to be accompanied with hysteresis,[6] which is a roadblock for achieving high-performance PVSCs.

Currently, the anti-solvent engineering method has been widely employed to prepare perovskite films.[7] Typically, the anti-solvent (e.g., chlorobenzene, toluene and ether) is dripped to remove most of the solvent of perovskite materials (e.g., dimethylformamide (DMF), dimethyl sulfoxide (DMSO)). As a result, an intermediate film (e.g., $CH_3NH_3PbI_3$:DMF) is formed.[8] After thermal annealing, the coordinated solvent molecules and other residual uncoordinated solvent are removed, which leaves the Pb atoms at the grain boundary uncoordinated.[9]

Some efforts have been put to reduce the defects concentrations in the formed perovskite films. For example, Huang *et al.* firstly found that depositing a fullerene layer on perovskite surface can effectively passivate the defects and eliminate the hysteresis effect.[10] Snaith *et al.* demonstrated that pyridine and thiophene were effective in passivating the trap states on the surface of perovskite films due to their interaction with the under-coordinated lead atoms.[11] Jen *et al.* proposed a series of bifunctional diammonium iodides to passivate perovskite surfaces and grain boundaries considering their bilateral ammonium iodide end simultaneously

passivated the perovskite layer and doped the adjacent electron-transporting layer (PCBM) in derived PVSCs.[12] Sun *et al.* employed the small molecule of boron subphthalocyanine chloride (SubPc) to passivate the defects by filling up the pinholes at the perovskite surface and grain boundaries.[13] Huang and co-workers employed a π-conjugated Lewis base (indacenodithiophene end-capped with 1.1-dicyanomethylene-3-indanone, IDIC) with n-type semiconductor property to the $CH_3NH_3PbI_3$ based solar cells as an interlayer between $CH_3NH_3PbI_3$ and cathode. The carbonyl and cyano groups of IDIC passivated the under-coordinated Pb of $CH_3NH_3PbI_3$ polycrystalline films through coordination between the Lewis acid and base.[14] Miyasaka *et al.* suggested that the hydrophobic polymer (poly(4-vinylpyridine) passivated the under-coordinated Pb atoms on the surface of perovskite by its pyridine Lewis base side chains and thereby eliminates surface-trap states and non-radiative recombination.[15] Recently, Huang *et al.* further discovered that π-conjugated Lewis base and quaternary ammonium halide can also passivate the defects of underlying perovskite layers.[16]

In addition, the incorporation of various additives (e.g., alkyl halide,[17] ionic liquid,[18] Lewis base,[19] alkali metal cations (e.g., K^+),[20] fullerene derivatives,[21] and polymers,[22]) into perovskite precursor solution is another strategy to manipulate the nucleation and growth process of perovskite films, and passivate the trap states. Although these strategies have been proven to effectively reduce the defects of perovskite films, a larger quantity of defects (e.g., uncoordinated Pb atoms) within the perovskite film still exist in conventional deposition method.

In this work, we propose a new strategy of simultaneously controlling the perovskite formation kinetics and reducing the defects (e.g., unsaturated Pb) in perovskite film. Interestingly, the incorporation of cyano-based small molecules into perovskite precursor solution can realize the strategy for forming densely packed perovskite films with low defect concentrations. Our results demonstrate that by using non-fullerene materials with cyano groups, inverted planar-structured PVSCs show significant PCE improvement to 20.10%,

View Article Online
DOI: 10.1039/C8TA08819E

which is among the highest values of low-temperature processed solar cells. This work provides a new strategy to further improve the film quality of low-temperature processed perovskite films and the relevant device performances.

2. Results and Discussion

2.1. Coordination between Pb and cyano-based small molecules

The cyano-based small molecules that we will study is non-fullerene materials including 3,9-bis(2-methylene-(3-(1,1-dicyanomethylene)-indanone)-5,5,11,11-tetrakis(4-hexylphenyl)-dithieno[2,3-d:2',3'-d']-s-indaceno[1,2-b:5,6-b']-dithiophene (ITIC, see Figure 1a)[23] and 2,2'-((2Z,2'Z)-(((4,4,9,9-tetrakis(4-hexylphenyl)-4,9-dihydro-s-indaceno[1,2-b:5,6-b']dithiophene-2,7-diyl)bis(4-((2-ethylhexyl)oxy)thiophene-5,2-diyl))bis(methanylylidene))bis(5,6-difluoro-3-oxo-2,3-dihydro-1H-indene-2,1-diylidene))dimalononitrile (IEICO-4F, see **Figure 1a**)[24]. It is because many non-fullerene materials are with cyano groups, which may have potential in contributing to coordinate with Pb atoms and modify the formation kinetics of perovskite. In addition, thanks to the high boiling point of non-fullerene materials, it cannot be easily removed during perovskite film formation, and thus can help to inhibit the defects formation. To unveil of the coordination between Pb atom and cyano-based small molecules of non-fullerene materials, we first study the color change of PbI_2 solution without and with the non-fullerene materials. Taking ITIC as an example here. Conventionally, the PbI_2 in DMF solution shows a pale yellow color as depicted in **Figure 1b**. When PbI_2 dissolved in ITIC:DMF saturated solution (The preparation method can be found in Experimental Section), a color of deep blue was obtained immediately for PbI_2:ITIC solution (blue-PbI_2:ITIC) as shown in **Figure 1c**. The color of deep blue is originated from the absorption of ITIC. Remarkably, after aged for 4 days, there is a dramatic change of the color of PbI_2:ITIC solution to orange-red (red-PbI_2:ITIC, **Figure 1d**) which indicates the coordination between PbI_2 and ITIC molecules.

To further clarify the coordination between PbI_2 and ITIC, photoluminescence (PL) measurement, fourier transform infrared (FTIR) spectroscopy, X-ray diffraction (XRD) and X-ray photoelectron spectroscopy (XPS) characterizations have been conducted. The PL of samples prepared onto quartz by the three kinds of solution discussed above through spin-coating is shown in **Figure 2a**. While the control PbI_2 film shows a PL peak centered at 550 nm, the blue-PbI_2:ITIC film exhibits two obvious peaks centered at 550 nm and 752 nm respectively. The emerged 752 nm peak is ascribed to ITIC, whose PL spectrum is as shown in **Figure S1**. After aging the blended solution for 4 days, the formed film shows distinct PL characteristics. Apparently, the peak centered at 725 nm is quenched, and a new peak centered at 633 nm emerges. This newly emerged peak is ascribed to ITIC coordinated PbI_2. The chemical interaction between PbI_2 and ITIC was also investigated by FTIR spectroscopy. As depicted in **Figure S2**, the stretching vibration of cyano (C≡N) shifts to a lower wavenumber (shifted from 2214 cm^{-1} to 2210 cm^{-1}) and the vibration strength for C≡N was weakened in PbI_2:ITIC film as compared to pristine ITIC film, indicating existence of interaction between PbI2 and ITIC.

Figure 2b shows the XRD patterns of the PbI_2 intermediate film (without annealing) formed from DMF solution and ITIC:DMF saturated solution. Typically, PbI_2 film shows (001), $(\bar{1}11)$ and $(0\bar{1}2)$ planes at 12.66°, 25.95° and 34.28° respectively.[25] The intermediate film from pure DMF solution shows two additional peaks at 8.96° and 9.54°, which are ascribed to (011) and (020) planes of DMF molecule coordinated PbI_2.[26] Interestingly, after blending with ITIC, this peak is diminished as shown in **Figure 2b**, indicating that the coordination by DMF is substituted by ITIC.

We further investigated the interaction between PbI_2 and ITIC and the composition of PbI_2:ITIC film by XPS characterization. As shown in **Figure 2c**, the PbI_2:ITIC film exhibit two peaks in the S 2p region, *i.e.* S $2p_{1/2}$ (164.4 eV) and S $2p_{3/2}$ (162.9 eV), which indicates the

existence of ITIC in the resultant film. In the Pb 4f region (see Figure 2d), both PbI_2 and PbI_2:ITIC films, the XPS spectra show two peaks centered at 143.4 eV and 138.4 eV, corresponding to Pb $4f_{5/2}$ and Pb $4f_{7/2}$ respectively. Besides, there are two satellite peaks shifted toward lower binding energy compared with the two main peaks, which are centered at 141.7 eV and 136.8 eV respectively. These two peaks are assigned to unsaturated Pb atoms.[27] Noteworthy, the satellite peaks in PbI_2 films are quite outstanding. The ratio between the satellite peak and corresponding main peak are 0.55:1 and 0.72:1 for Pb $4f_{5/2}$ and Pb $4f_{7/2}$ respectively. While the ratios decrease to 0.04:1 and 0.15:1 respectively for PbI_2:ITIC film. This prominent decreasing in the ratio of saturated and unsaturated Pb atoms indicates the amount of unsaturated Pb atoms is substantially suppressed.

2.2. Perovskite formation assisted by cyano-based small molecule

Employing the interaction between ITIC and PbI_2, we realize strategy for forming high-quality perovskite films by simply adding the non-fullerene material with cyano group into perovskite precursor solution. Different amounts of ITIC (*i.e.* 0, 0.125, 0.25, 0.5, 1 and 2 mg respectively), 500 mg PbI_2, 190 mg CH_3NH_3I and 30 mg $PbCl_2$ were stirred together for 3 h, followed by filtering using a 0.2 μm PTFE filter. After filtering, the precursor solution became clear and displayed different colors as shown in **Figure 3a**. With the increasing of added ITIC, the color changes from pale yellow to wine red gradually. This color transition is similar with the case of ITIC added PbI_2:ITIC solution, which is ascribed to the formed PbI_2:ITIC complex. The optical properties of the perovskite precursor solution have been investigated as shown in **Figure 3b**. Due to the formation of PbI_2:ITIC complex, an additional absorption appears in the range of 460 - 600 nm. Moreover, we have measured PL spectra of ITIC, perovskite, and perovskite:ITIC solution as shown in **Figure 3c**. The blue ITIC solution has a major PL peak at 784 nm, and the yellow control perovskite solution has a PL peak at 560 nm which is consistent with previously reported values.[28] Interestingly, the peak at 784 nm is quenched and the peak at 560 nm partially remains in the perovskite solution after adding the ITIC additive.

View Article Online
DOI: 10.1039/C8TA08819E

At the same time, a new peak at 621 nm, appears in the PL spectra of perovskite:ITIC solution. This new peak persuades us to believe that a new complex exists in the perovskite:ITIC solution.

Considering the Lewis base characteristic of ITIC and Lewis acidic characteristic of PbI_2, we further study the possibilities of forming PbI_2-ITIC complex from PbI_2 and ITIC in the solution. This complex absorbs light in the range of 460-600 nm and emits light which centers at 621 nm. ITIC, which binds with positively charged under-coordinated Pb^{2+} ions could passivate the defects in the final perovskite active layer, contributes to photovoltaic performance enhancement of perovskite solar cells as discussed below.

We prepare perovskite films by spin-coating the perovskite precursor solutions on the NiO_x/ITO substrate and using chlorobenzene as the anti-solvent (see Experiment Section). The X-ray diffraction (XRD) results (**Figure 3d**) show that the crystallinity of perovskite films with and without ITIC molecules are similar. We also study the morphology of perovskite prepared from the precursor without and with ITIC as depicted in **Figure 3e,f**. It is clearly shown that ITIC incorporated perovskite film has a more compact morphology and larger gain size (**Figure S3)** than the control samples. The densely packed perovskite film can be explained by the better connectivity between adjacent crystallites, leading to a more efficient pathway for carrier transport and suppressed charge recombination.

The enhanced morphology of perovskite film by incorporation of cyano-based small molecule can be explained from the classic nucleation and grain growth theory. Typically, in perovskite formation, a "heterogeneous" nucleation process accompanies with grain growth in 3D following Volmer-Weber growth mode. The size of the crystal depends on the nucleation rate (N) and growth rate (G) following the equation $z_s = (\frac{N}{G})^{1/2}$, where z_s is the number of grains per unit area, which is inversely proportional to the grain size. In this study, since the cyano-based small molecules partially coordinate PbI_2 in the precursor solution, which can reduce the nucleation rate and facilitate the perovskite grain growth due to the quick removal of solvents

View Article Online
DOI: 10.1039/C8TA08819E

(DMF). The combined effects consequently lead to a decreased z_s, and densely packed morphology in the cyano-based small molecule incorporated perovskite film.

2.3. Device Performances

We have fabricated p-i-n planar PVSCs with configuration of ITO/NiO_x/$CH_3NH_3PbI_{3-x}Cl_x$/C_{60}/BCP/Ag (see **Figure 4a**), where room-temperature solution-processed NiO_x nanostructure, C_{60}, and bathocuproine (BCP) as hole transport layer, electron transport layer, and interface layer, respectively. The corresponding energy-level diagram of the devices is illustrated in **Figure S4**. As shown in **Figure 4b** and **Table 1**, the control device (without non-fullerene material incorporation) showed typical performance with short circuit current density (J_{sc}) of 21.61 mA cm^{-2}, open circuit voltage (V_{oc}) of 1.06 V, fill factor (FF) of 0.78, PCE of 17.81%. In striking contrast, the PVSCs with ITIC incorporation (The optimized concentration of ITIC is 2 mg/ml, see **Table S1**) show a significantly improved performance with J_{sc} of 22.80 mA cm^{-2}, V_{oc} of 1.09 V, FF of 0.81, PCE of 20.10%. Both the control device and ITIC-incorporated PVSCs showed negligible hysteresis. The IPCE of the fabricated devices (without and with ITIC) is presented in **Figure 4c**. The integrated J_{SC} values are 20.51 and 21.79 mA cm^{-2} respectively, which is consistent with the enhancement of J_{SC} derived from the *J-V* characteristics. To further confirm the improvement of photovoltaic performances in perovskite:ITIC-based PVSCs, more separate devices were fabricated and tested. The histograms of the device efficiencies are presented in **Figure 4d**. The ITIC:perovskite-based PVSCs show an average PCE of 19.0%, higher than that of control devices (17.25%). We also verify our strategy in another non-fullerene material with cyano group of IEICO-4F. As shown in **Table 1** and **Figure S5**, the usage of IEICO-4F can also improve the PCE of PVSCs up to 19.13% ($PCE_{avg.}$=18.66%). By using solution processable $PC_{61}BM$ as ETL, all-solution processed PVSCs with average PCE over 15% can be achieved (**Figure S6** and **Table S2**).

2.3 Contributions of cyano-based small molecules

To understand the PCE improvement by incorporating those non-fullerene materials with cyano group, we further investigate the optical and electronic properties of perovskite films and their device physics. As shown in **Figure 5**, the cyano group of the small molecules (i.e. non-fullerene materials) can coordinate with unsaturated Pb atoms in the perovskite film while DMF will evaporate and thus de-coordinate during the annealing process. As a result, cyano-based small molecule contained perovskite would typically have less concentration of unsaturated Pb atoms, *i.e.* defects, which contributes to the enhancement of photovoltaic performances. We have also investigated the XPS of Pb 4f of the resultant perovskite film formed by incorporating ITIC into the perovskite precursor as shown in **Figure 6**a. Similar to our discovery in the PbI_2:ITIC films described above, the satellite peaks are substantially weakened after the coordination effect of ITIC. Quantitatively, the peak area ratio between the satellite peak (140.4 eV) and Pb $4f_{5/2}$ main peak(142.2 eV) decreases from 0.064:1 to 0.038:1, while the peak area ratio between the corresponding satellite peak (135.7 eV) and Pb $4f_{7/2}$ main peak (137.3 eV) decreases from 0.15:1 to 0.11:1. This substantial reduction of satellite peaks' area substantiates the reduced concentration of unsaturated Pb atoms in the perovskite film after the addition of ITIC.

The photocarrier dynamics is studied by steady-state photoluminescence (PL) as shown in **Figure 6b**. All the perovskite films with different concentrations of ITIC show a PL peak centered at 765 nm. Compared with pristine perovskite film, the PL intensity of perovskite:ITIC based films is gradually weakened with the increase of the concentration of ITIC. With respect to the pristine perovskite film, the PL quenching ratio is calculated to be 75% when ITIC is added (2 mg mL^{-1}). This quenching indicates more efficient carrier extraction instead of radiative recombination within the perovskite film. The more efficient carrier extraction is further confirmed by time-resolved PL (TRPL) measurements as shown in **Figure 6c**. The fitting results are as shown in **Table 2**. The reference film exhibits an average carrier extraction time of 200 ns while the value decreases to 61 ns for perovskite:ITIC film.

View Article Online
DOI: 10.1039/C8TA08819E

The defect density within the perovskite film is determined by fabricating hole-only devices with the structure of ITO/NiO_x/$CH_3NH_3PbI_{3-x}Cl_x$ or $CH_3NH_3PbI_{3-x}Cl_x$:ITIC/MoO_3/Ag. The *J-V* characteristics of the hole-only device are as shown in **Figure 6d**. The *J-V* curve typically displays three regions, *i.e.* an ohmic region at low bias, a trap-filling (TFL) region at medium bias and a trap-free space charge limit current (SCLC) region. The defects density (N_d) within the perovskite film is closely related to the trap-filled limit voltage (V_{TFL}) by the equation $N_d = \frac{2\varepsilon_0\varepsilon_r V_{TFL}}{qL^2}$, where ε_0 and ε_r are vacuum permittivity and relative permittivity of the perovskite respectively, V_{TFL} is the onset voltage determined from the *J-V* curve, q is the elementary charge and L is the thickness of the perovskite film. The defects density is calculated to be 1.66×10^{16} cm^{-3} and 1.23×10^{16} cm^{-3} within the perovskite and perovskite:ITIC films respectively, which proves that the concentration of unsaturated Pb atoms is diminished after the coordination engineering.

Electrical impedance spectroscopy (EIS) is a powerful tool to understand the carrier dynamics in solar cells. As shown in **Figure 6e,f**, the ITIC- incorporated PVSC exhibits a much larger recombination resistance (R_{rec}) and longer electron lifetime at different voltage biases than that of the control devices, which indicates the ITIC-incorporation effectively reduces the recombination paths and thus energy losses. To further explore the charge transfer and recombination dynamics in devices, photocurrent (TPC) and transient photovoltage (TPV) measurements were conducted. The TPV and TPC measurements were performed under 0.5 sun illumination, excited by a 532 nm 6 ps pulse laser with certain intensity, and the data are fitted by exponential decay function. As shown in **Figure S7a**, the ITIC- incorporated PVSCs with ITIC yield a larger photocurrent with a shorter charge transfer time (0.80 μs) compared with the control devices (1.06 μs), indicating improved electron transport and charge collection. From the TPV measurement (**Figure S7b**), the ITIC- incorporated PVSCs exhibit a photovoltage decay time of 0.52 μs, which is longer than that of the control devices without

ITIC (0.43 μs). The prolonged lifetime suggests that less carrier recombination takes place in the devices with ITIC incorporation. Therefore, ITIC incorporation strategy significantly improves the film quality of perovskites and thus device performances.

3. Conclusion

In summary, we realize the strategy of simultaneously control the perovskite formation kinetics and inhibit the defects formation in perovskite film. The strategy is demonstrated through the incorporation of non-fullerenes with cyano group into perovskite precursor solution. As a result, densely packed perovskite films with low defect concentrations can be formed. By using the strategy, the PCE of low-temperature processed PVSCs is significantly improved from ~18% to over 20%. This work provides a new scheme to simultaneously control the perovskite formation kinetics and defect density, which paves the way to further improve the performance of perovskite optoelectronic devices.

4. Experimental Section

Materials: All materials were purchased and used as received. Lead (II) iodide (PbI_2, 99.99%, trace metals basis) was purchased from Shenzhen Dieckmann Technology Development co., Ltd. Methylammonium iodide (MAI, >99%) was purchased from Dyesol Pty Ltd. Lead (II) chloride ($PbCl_2$, 99.999%, trace metals basis) was purchased from Sigma-Aldrich. N,N-Dimethylformamide (DMF, extra dry, 99.8%), chlorobenzene (CB, extra dry, 99.8%) and bathocuproine (BCP, 98%) were purchased from Acros Organics. C_{60} (99%) was purchased from Nichem Fine Technology Co. Ltd. ITIC and and $PC_{61}BM$ were purchased from Solarmer Co., Ltd. IEICO-4F was synthesized according to our previous report.[18]

Device Fabrication: Indium tin oxide (ITO) coated glass substrates with sheet resistance of 15 Ω sq^{-1} were cleaned by a standard procedure with detergent, acetone and ethanol ultrasonic bath for each of 10 min in sequence. The cleaned ITO-coated glasses were UVO treated for 20

min. NiO_x HTLs were deposited by a reported post-treatment-free method.[29] The perovskite precursor solution was prepared by stirring 500 mg PbI_2, 190 mg MAI and 30 mg $PbCl_2$ in 1 mL DMF. The perovskite:ITIC precursor solution was prepared by stirring 2 mg ITIC, 500 mg PbI_2, 190 mg MAI and 30 mg $PbCl_2$ in 1 mL DMF. The precursor solution was stirred overnight and filtered before use. During the device fabrication process, 40 μL precursor solution was dropped onto NiO_x HTL followed by a spin-coating process at 5000 rpm for 20 s. 0.2 mL CB was spun onto the rotating precursor film at 5 s. After this anti-solvent drop-casting process, the films were annealed at 100 ^oC for 10 min. Then the perovskite or perovskite:ITIC films were transferred into vacuum chamber at a vacuum level of 3×10^{-6} Torr. C_{60} (20 nm) and BCP (7 nm) were thermally evaporated in sequence with a deposition rate of 0.5 Å/s or $PC_{61}BM$ (20 mg ml^{-1} in dichlorobenzene) was spin-coated onto the perovskite or perovskite:ITIC films. Finally, Ag (100 nm) were thermally evaporated through a shadow mask as the top cathode, which defined the device area as 6 mm^2.

Characterization: The XRD spectrum was obtained using D5005 X-ray diffraction system (CuKα radiation, λ = 1.54056 Å). UV-vis absorption spectra were obtained from a home-build system with a xenon lamp as a light source and an integrated sphere associated with charge-coupled device (Ocean Optics QE Pro) as a detector. X-ray photoelectron spectroscopy (XPS) of perovskite films was measured in the ultrahigh vacuum environment using Physical Electronics PHI 5802 with a monochromatic Al Kα X-ray source. The *J-V* curves were recorded from 0→1.2 V or 1.2→0 V using a Keithley 2635 apparatus with scan rate being 0.10 V s^{-1}. Solar-simulated AM 1.5 sunlight was generated using a Newport AM 1.5G irradiation (100 mW/cm^2), calibrated with an ISO 17025-certified KG3-filtered silicon reference cell. The spectral mismatch factor was calculated to be less than 1%. The scan speeds for all *J-V* curves are 0.10 mV/s. To avoid the side edge effect, a black mask with an aperture area of 6 mm^2 was employed during the *J-V* measurement. The IPCE measurement was performed by a system combining xenon lamp, a monochromator (SpectraPro-2150i, Acton Research Corporation), a

chopper, two optical filters (320 and 570 nm), and a lock-in amplifier (SR830, Stanford Research Systems) together with a calibrated silicon photodetector (Hamamatsu mono-Si cell). PL measurement was conducted by PicoQaunt FluoTime 300. The excitation light wavelength is 375 nm. A picosecond 375 nm pulse laser (LDH-P-C-375) with a pulse width of <40 ps and a repetition rate of 5 MHz was used to excite the perovskite. SEM images were measured by using a Hitachi S-4800 FEG scanning electron microscope. The impedance measurement was carried out by Zahner electrochemistry station (Zennium Pro) with a DC bias of 0.1 V and a frequency range from 1 Hz and 1 MHz with AC amplitude of 10 mV under illumination with white LED array. TPC and TPV measurements were conducted with a 532 nm 6 ps pulse width laser (130 μJ per pulse at 100 Hz) and recorded by a 4 GHz Keysight MSO9404A digital oscilloscope. TPV measurements were conducted by using the same laser and oscilloscope under 0.5 sun illumination. Lifetime values were extracted by using an exponential decay fitting. The FTIR spectra (500-4,000 cm^{-1}) were recorded on a JASCO FT/IR-6100 spectrophotometer.

Acknowledgements

J.C. and H.Z. contributed equally to this work. This work was supported by the University Grant Council of the University of Hong Kong (Grant 104003113, 201711159074, 102009639), the General Research Fund (Grants 17211916, 17204117 and 17200518). J.H. would like to acknowledge the financial support from the National Natural Science Foundation of China (Nos. 2170040201, 51673201). We thank Shishir Venkatesh and Vellaisamy A. L. Roy from City University of Hong Kong, for their help in XRD and XPS characterizations. We also appreciate Kai Wang and Aung Ko Ko Kyaw from Southern University of Science and Technology for their help in device fabrication during the revision process.

References

[1] a) M. Saliba, T. Matsui, K. Domanski, J.-Y. Seo, A. Ummadisingu, S. M. Zakeeruddin, J.-P. Correa-Baena, W. R. Tress, A. Abate, A. Hagfeldt, *Science* **2016**, 354, 206; b) W. J. Yin, T. Shi, Y. Yan, *Adv. Mater.* **2014**, 26, 4653; c) H. Chen, F. Ye, W. Tang, J. He, M. Yin, Y. Wang, F. Xie, E. Bi, X. Yang, M. Grätzel, *Nature* **2017**, 550, 92; d) H. Zhang, J. Cheng, D. Li, F. Lin, J. Mao, C. Liang, A. K. Y. Jen, M. Grätzel, W. C. Choy, *Adv. Mater.* **2017**, 29, 1604695.
[2] W. S. Yang, B.-W. Park, E. H. Jung, N. J. Jeon, Y. C. Kim, D. U. Lee, S. S. Shin, J. Seo, E. K. Kim, J. H. Noh, *Science* **2017**, 356, 1376.
[3] a) W.-J. Yin, T. Shi, Y. Yan, *Appl. Phys. Lett.* **2014**, 104, 063903; b) W. E. Sha, X. Ren, L. Chen, W. C. Choy, *Appl. Phys. Lett.* **2015**, 106, 221104.
[4] J. M. Ball, A. Petrozza, *Nat. Energy* **2016**, 1, 16149.
[5] B. Wu, H. T. Nguyen, Z. Ku, G. Han, D. Giovanni, N. Mathews, H. J. Fan, T. C. Sum, *Adv. Energy Mater.* **2016**, 6, 1600551.
[6] D. Zhao, M. Sexton, H.-Y. Park, G. Baure, J. C. Nino, F. So, *Adv. Energy Mater.* **2015**, 5, 1401855.
[7] a) N. J. Jeon, J. H. Noh, Y. C. Kim, W. S. Yang, S. Ryu, S. I. Seok, *Nat. Mater.* **2014**, 13, 897; b) M. Saliba, T. Matsui, J.-Y. Seo, K. Domanski, J.-P. Correa-Baena, M. K. Nazeeruddin, S. M. Zakeeruddin, W. Tress, A. Abate, A. Hagfeldt, *Energy Environ. Sci.* **2016**, 9, 1989; c) D. Zhao, Y. Yu, C. Wang, W. Liao, N. Shrestha, C. R. Grice, A. J. Cimaroli, L. Guan, R. J. Ellingson, K. Zhu, *Nat. Energy* **2017**, 2, 17018; d) S. Shao, J. Liu, G. Portale, H. H. Fang, G. R. Blake, G. H. ten Brink, L. J. A. Koster, M. A. Loi, *Adv. Energy Mater.* **2018**, 8, 1702019.
[8] F. Hao, C. C. Stoumpos, Z. Liu, R. P. Chang, M. G. Kanatzidis, *J. Am. Chem. Soc.* **2014**, 136, 16411.
[9] J. S. Manser, M. I. Saidaminov, J. A. Christians, O. M. Bakr, P. V. Kamat, *Acc. Chem. Res.* **2016**, 49, 330.
[10] a) Y. Shao, Z. Xiao, C. Bi, Y. Yuan, J. Huang, *Nat. Commun.* **2014**, 5, 5784; b) Y. Lin, L. Shen, J. Dai, Y. Deng, Y. Wu, Y. Bai, X. Zheng, J. Wang, Y. Fang, H. Wei, W. Ma, X. C. Zeng, X. Zhan, J. Huang, *Adv. Mater.* **2017**, 29, 1604545.
[11] N. K. Noel, A. Abate, S. D. Stranks, E. S. Parrott, V. M. Burlakov, A. Goriely, H. J. Snaith, *ACS Nano* **2014**, 8, 9815.
[12] T. Zhao, C.-C. Chueh, Q. Chen, A. Rajagopal, A. K.-Y. Jen, *ACS Energy Lett.* **2016**, 1, 757.
[13] M. Xu, J. Feng, X.-L. Ou, Z.-Y. Zhang, Y.-F. Zhang, H.-Y. Wang, H.-B. Sun, *IEEE Photonics J.* **2016**, 8, 1.
[14] Y. Lin, L. Shen, J. Dai, Y. Deng, Y. Wu, Y. Bai, X. Zheng, J. Wang, Y. Fang, H. Wei, *Adv. Mater.* **2017**, 29, 1604545.
[15] B. Chaudhary, A. Kulkarni, A. K. Jena, M. Ikegami, Y. Udagawa, H. Kunugita, K. Ema, T. Miyasaka, *ChemSusChem* **2017**, 10, 2473.
[16] X. Zheng, B. Chen, J. Dai, Y. Fang, Y. Bai, Y. Lin, H. Wei, Xiao C. Zeng, J. Huang, *Nat. Energy* **2017**, 2, 17102.
[17] C.-C. Chueh, C.-Y. Liao, F. Zuo, S. T. Williams, P.-W. Liang, A. K. Y. Jen, *J. Mater. Chem. A* **2015**, 3, 9058.
[18] J.-Y. Seo, T. Matsui, J. Luo, J.-P. Correa-Baena, F. Giordano, M. Saliba, K. Schenk, A. Ummadisingu, K. Domanski, M. Hadadian, A. Hagfeldt, S. M. Zakeeruddin, U. Steiner, M. Grätzel, A. Abate, *Adv. Energy Mater.* **2016**, 6, 1600767.
[19] J.-W. Lee, H.-S. Kim, N.-G. Park, *Acc. Chem. Res.* **2016**, 49, 311.
[20] M. Abdi-Jalebi, Z. Andaji-Garmaroudi, S. Cacovich, C. Stavrakas, B. Philippe, J. M. Richter, M. Alsari, E. P. Booker, E. M. Hutter, A. J. Pearson, S. Lilliu, T. J. Savenije, H. Rensmo, G. Divitini, C. Ducati, R. H. Friend, S. D. Stranks, *Nature* **2018**, 555, 497.

[21] J. Xu, A. Buin, A. H. Ip, W. Li, O. Voznyy, R. Comin, M. Yuan, S. Jeon, Z. Ning, J. J. McDowell, P. Kanjanaboos, J.-P. Sun, X. Lan, L. N. Quan, D. H. Kim, I. G. Hill, P. Maksymovych, E. H. Sargent, *Nat. Commun.* **2015**, 6, 7081.
[22] C.-C. Zhang, M. Li, Z.-K. Wang, Y.-R. Jiang, H.-R. Liu, Y.-G. Yang, X.-Y. Gao, H. Ma, *J. Mater. Chem. A* **2017**, 5, 2572.
[23] W. Zhao, D. Qian, S. Zhang, S. Li, O. Inganäs, F. Gao, J. Hou, *Adv. Mater.* **2016**, 28, 4734.
[24] H. Yao, Y. Cui, R. Yu, B. Gao, H. Zhang, J. Hou, *Angew. Chem. Int. Ed.* **2017**, 56, 3045.
[25] S. Luo, W. Daoud, *Materials* **2016**, 9, 123.
[26] H. Zheng, W. Wang, S. Yang, Y. Liu, J. Sun, *RSC Adv.* **2016**, 6, 1611.
[27] R. Lindblad, D. Bi, B.-w. Park, J. Oscarsson, M. Gorgoi, H. Siegbahn, M. Odelius, E. M. J. Johansson, H. Rensmo, *J. Phys. Chem. Lett.* **2014**, 5, 648.
[28] a) H. Yao, R. Yu, T. J. Shin, H. Zhang, S. Zhang, B. Jang, M. A. Uddin, H. Y. Woo, J. Hou, *Adv. Energy Mater.* **2016**, 6, 1600742; b) J. F. Condeles, R. A. Ando, M. Mulato, *J. Mater. Sci.* **2008**, 43, 525.
[29] H. Zhang, J. Cheng, F. Lin, H. He, J. Mao, K. S. Wong, A. K.-Y. Jen, W. C. Choy, *ACS Nano* **2016**, 10, 1503.

View Article Online
DOI: 10.1039/C8TA08819E

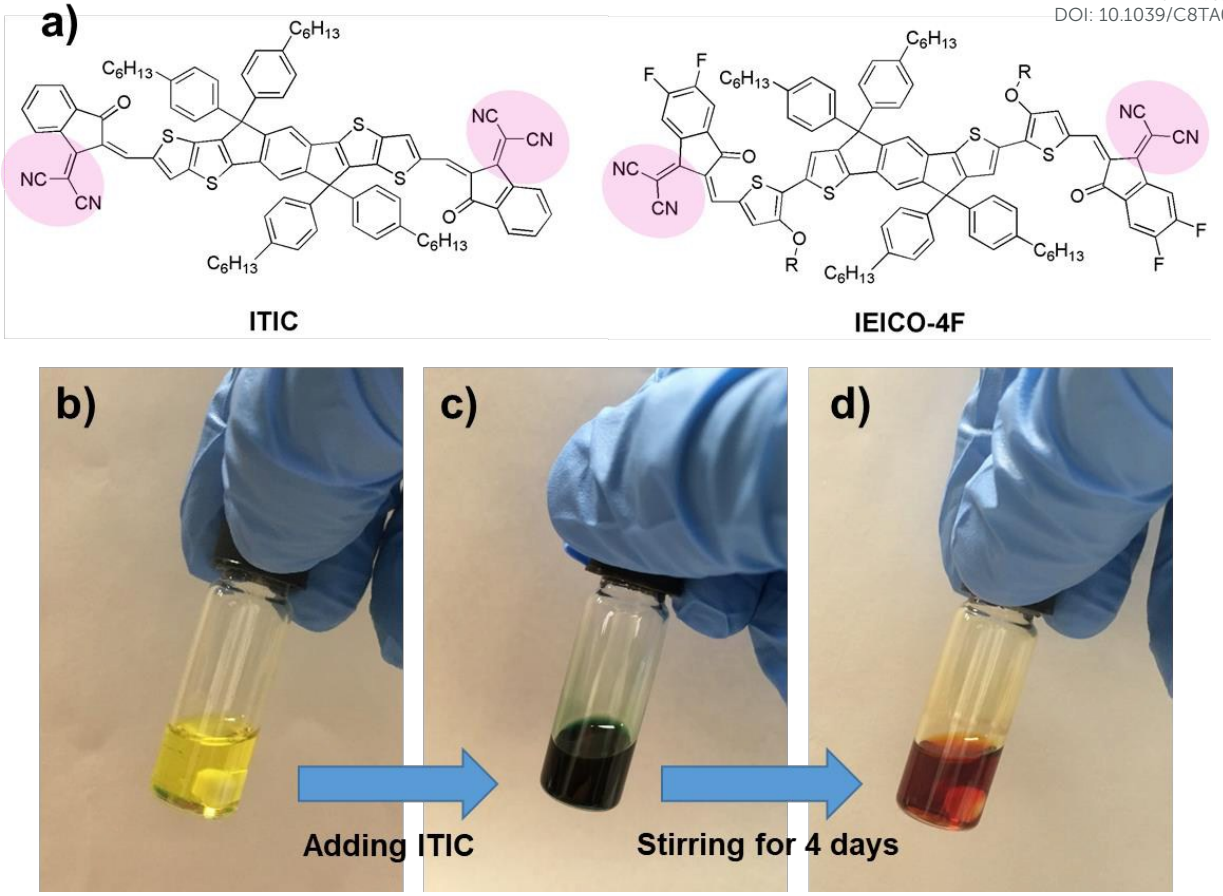

Figure 1. a) Molecular structure of cyano-based small molecules in this work. Photographs of b) PbI_2 solution; c) blue-PbI_2:ITIC solution; d) red-PbI_2:ITIC solution.

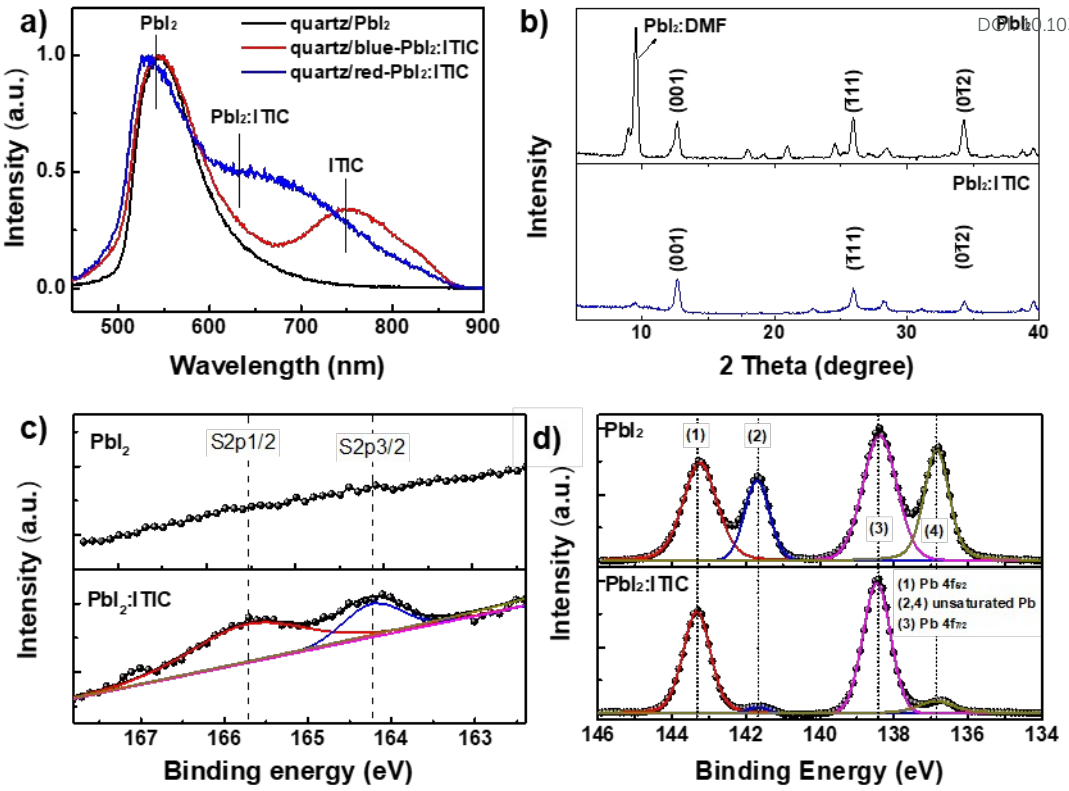

Figure 2. a) PL spectra of PbI_2, blue-PbI_2:ITIC and red-PbI_2:ITIC films on quartz substrates. b) XRD spectra of PbI_2 and red-PbI_2:ITIC films on ITO/NiO_x substrates. XPS spectra of c) S 2p and d) Pb 4f region of PbI_2 and red-PbI_2:ITIC films on ITO/NiO_x substrates.

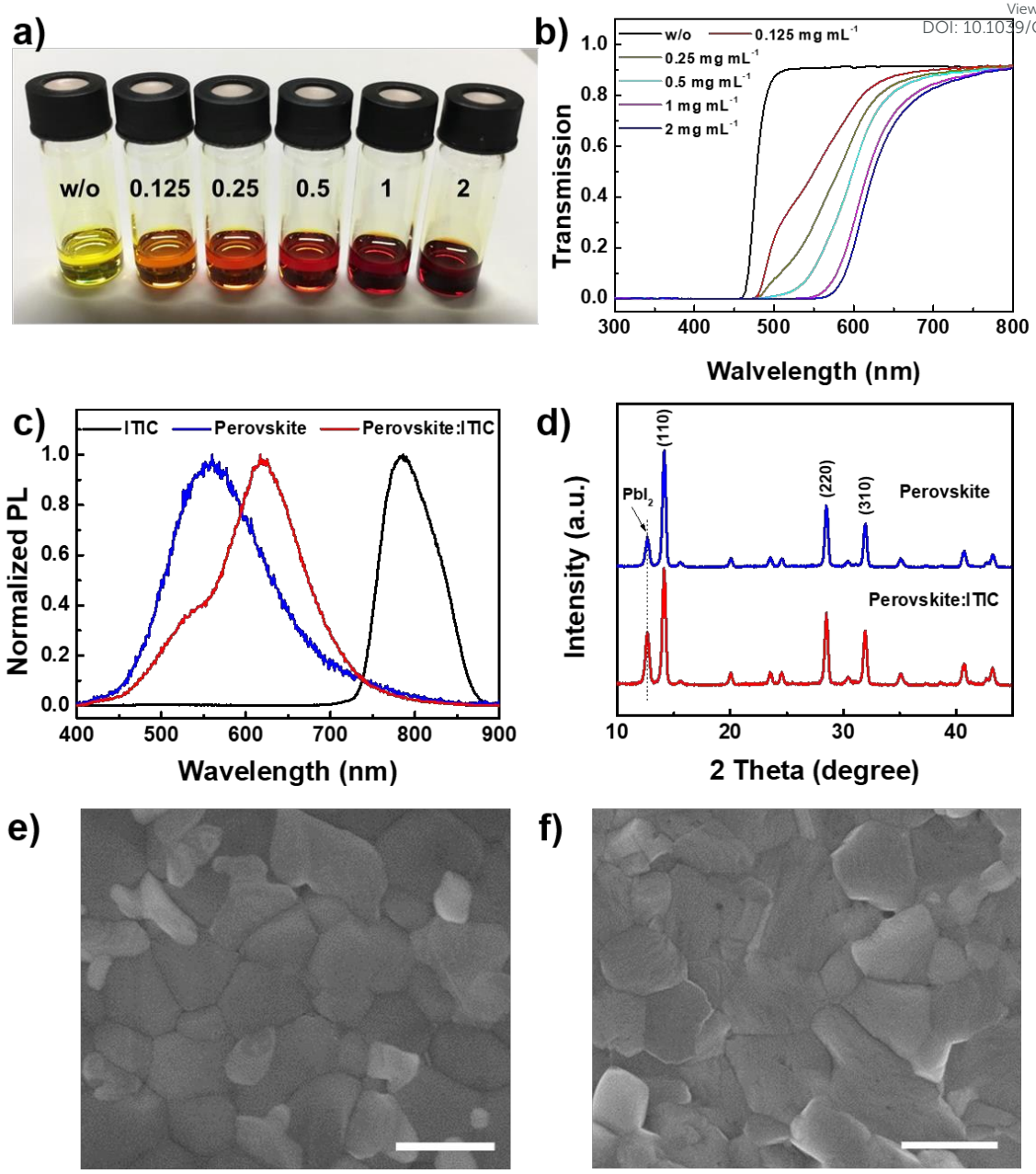

Figure 3. a) Photographs of perovskite and perovskite:ITIC precursor solutions (0.125 mg mL^{-1}, 0.25 mg mL^{-1}, 0.5 mg mL^{-1}, 1 mg mL^{-1}, and 2 mg mL^{-1}). b) Transmission spectra of perovskite and perovskite:ITIC precursor solution with different amount of added ITIC. c) Normalized PL spectra of ITIC solution, perovskite precursor solution and perovskite:ITIC precursor solution. d) XRD pattern of perovskite and perovskite:ITIC films. Top-view SEM images of e) perovskite and f) perovskite:ITIC films. The scale bar is 500 nm.

View Article Online
DOI: 10.1039/C8TA08819E

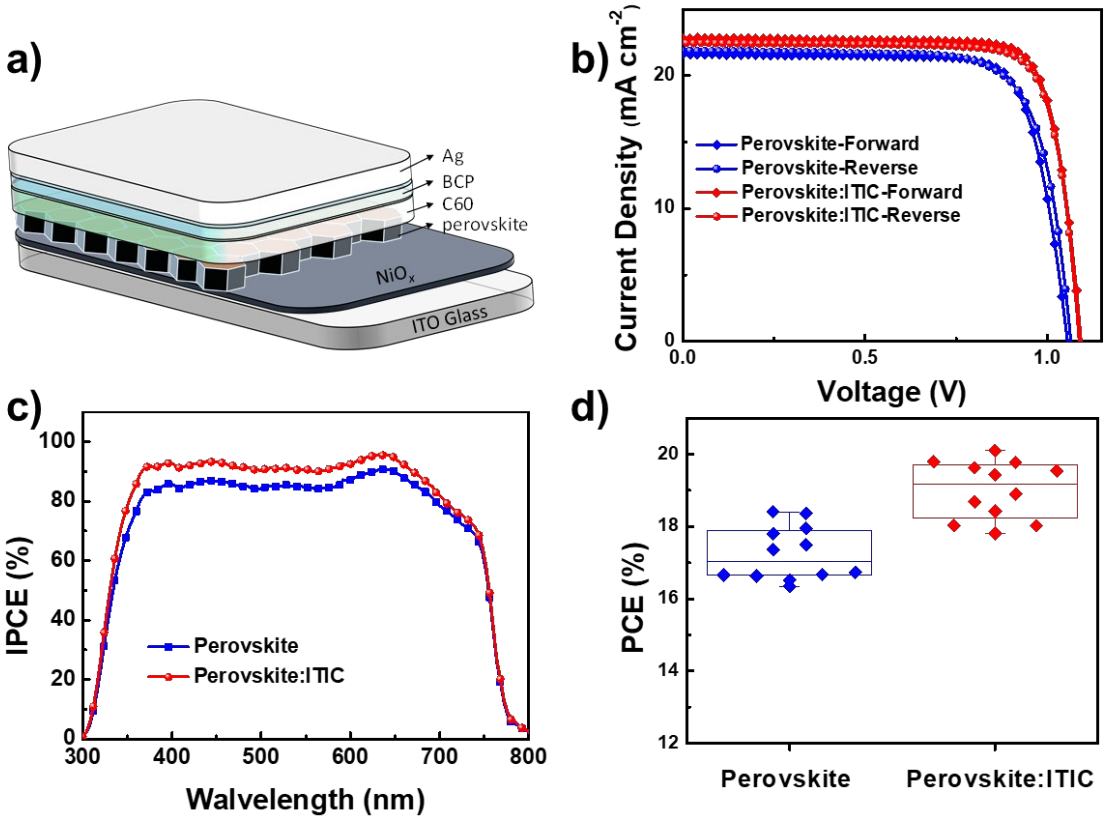

Figure 4. a) Schematic illustration of the structure of fabricated perovskite solar cells. b) Representative *J-V* curves, c) IPCE spectra, and d) statistics of the device efficiencies of perovskite and perovskite:ITIC based solar cells.

View Article Online
DOI: 10.1039/C8TA08819E

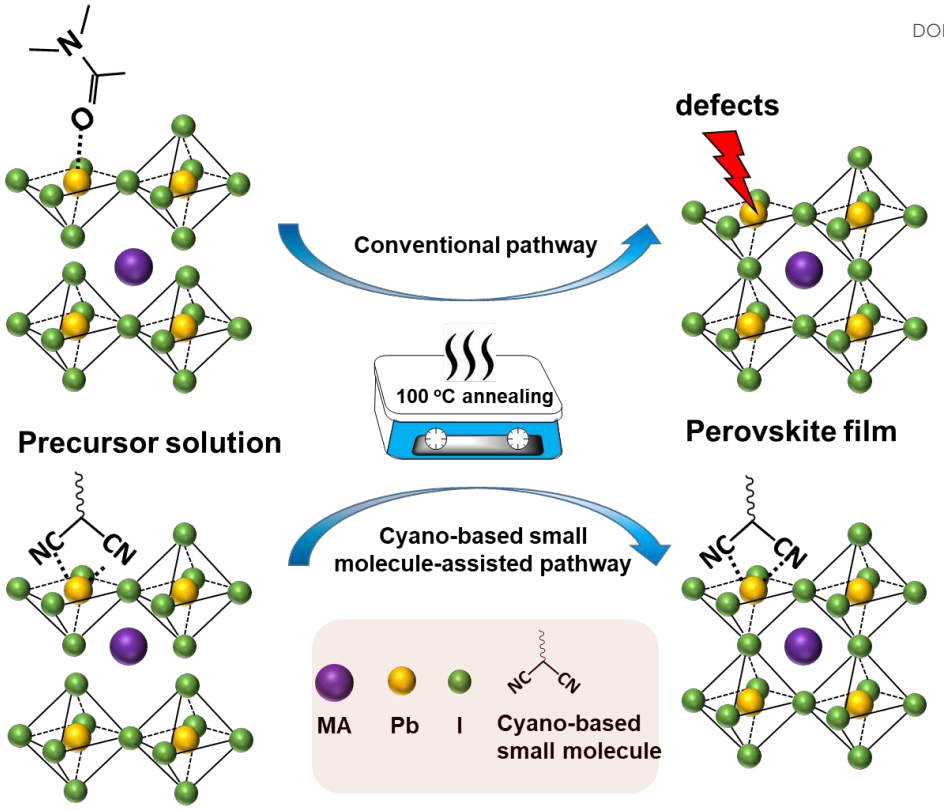

Figure 5. Schematic illustration of defect formation in perovskite crystal via conventional anti-solvent method and our cyano-based small molecule assisted strategy.

View Article Online
DOI: 10.1039/C8TA08819E

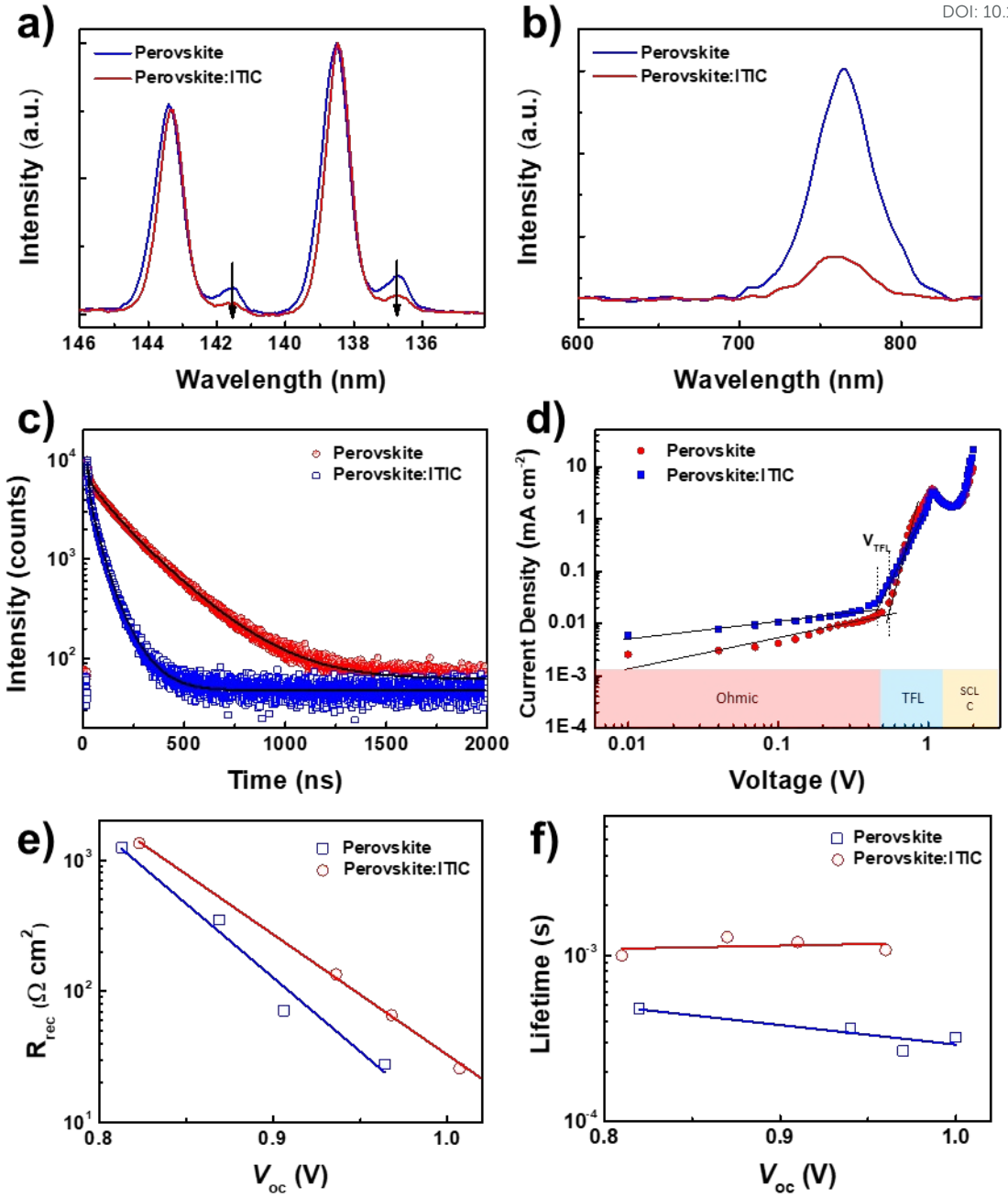

Figure 6. a) XPS spectra of Pb 4f region of perovskite and perovskite:ITIC films. b) Steady-state PL spectra of perovskite and perovskite:ITIC films deposited on ITO/NiO_x substrates; c) *J-V* characteristics of hole-only devices with a structure of ITO/ NiO_x/perovskite or perovskite:ITIC/MoO_3/Ag. Plots of e) interfacial resistance and f) lifetime as a function of applied voltage bias obtained from impedance spectroscopy under illumination.

View Article Online
DOI: 10.1039/C8TA08819E

Table 1. The photovoltaic parameters obtained from *J-V* characteristics of PVSCs with and without non-fullerene incorporation.

Non-fullerene with cyano group		J_{SC} (mA cm^{-2})	*Calculated* J_{SC} (mA cm^{-2})	V_{OC} (V)	FF	PCE (%)
w/o	Champion-F	21.61	20.51	1.06	0.78	17.81
	Champion-R	21.87		1.06	0.76	17.62
	Average	20.90± 0.48		1.05 ± 0.01	0.78 ± 0.01	17.25 ± 0.58
ITIC (2mg/ml)	Champion-F	22.80	21.79	1.09	0.81	20.10
	Champion-R	22.47		1.09	0.80	19.62
	Average	22.73±0.68		1.06±0.01	0.79±0.01	19.00±0.81
IEICO-4F(2mg/ml)	Champion-F	22.44		1.07	0.80	19.13
	Champion-R	22.50		1.07	0.79	18.96
	Average	22.13±0.34		1.07±0.01	0.79±0.01	18.66±0.37

a) Calculated J_{sc} from IPCE spectra; b) F= forward scan; R= reverse scan.

Table 2. Fitting results of the TRPL measurements of perovskite and perovskite:ITIC films.

	A_1 (cnts)	τ_1 (ns)	A_2 (cnts)	τ_2 (ns)	A_3 (cnts)	τ_3 (ns)	τ_{ave} (ns)
Perovskite	4103.8	230	2853	7.70	2176.9	98	200
Perovskite:ITIC	3598.1	41	3820	6.70	1261.9	96	61

Table of Contents

Incorporation of non-fullerene acceptor into perovskite precursor solution is demonstrated to form high-quality perovskite films with low defect concentrations. The power conversion efficiency of low-temperature processed perovskite solar cells is improved up to 20.10%.